Simultaneous Multicolor Fluorescence Cross-Correlation Spectroscopy to Detect Higher Order Molecular Interactions Using Single Wavelength Laser Excitation

Ling Chin Hwang,*† Michael Gösch,† Theo Lasser,† and Thorsten Wohland*
*National University of Singapore, Department of Chemistry, Singapore 117543, Singapore; and †Ecole Polytechnique Fédérale de Lausanne, Laboratoire d'Optique Biomédicale, CH-1015 Lausanne, Switzerland

ABSTRACT Fluorescence cross-correlation spectroscopy is a powerful method for the study of molecular interactions and dynamics in solution and even in living cells. Usually, in the optical setup, either two laser beams have to be superimposed in their respective confocal volumes or two-photon excitation is used for a dual-color detection system. It has been shown recently that fluorescence cross correlation can be achieved with spectrally similar fluorophores using single wavelength excitation fluorescence cross-correlation spectroscopy (SW-FCCS). In this study, we show that SW-FCCS allows the simultaneous excitation of up to three fluorophores in which the cross correlation of their fluctuation signals is detected separately in three detection channels. The experimental and theoretical model to describe triple pairwise cross correlations incorporating cross talk and possible changes in emission characteristics such as quenching upon binding are outlined. The effectiveness of SW-FCCS to detect binding of three interacting partners is experimentally verified with a standard ligand-receptor model, biotin-streptavidin, where differently labeled biotin ligands and their binding to a third-color labeled streptavidin are studied. The cross-correlation amplitudes and their changes with stoichiometric binding are analyzed and the upper limits of dissociation constants are determined. Performed with appropriate negative controls, SW-FCCS can determine interaction patterns between ligands and receptors.

INTRODUCTION

Fluorescence correlation spectroscopy (FCS) was introduced three decades ago to measure intensity fluctuations of fluorescent particles diffusing through a focused laser beam to obtain information such as translational diffusion coefficients and chemical rate constants (1–3). The improvement of this technique to single-molecule sensitivity was achieved by using a confocal microscope system with a high numerical aperture objective and single photon counting avalanche photodiodes as detectors (4,5). Since then, it has become an increasingly popular technique for the study of kinetics at thermodynamic equilibrium. Besides being able to determine the concentration and diffusion characteristics of the component measured (6), it has also been used to measure receptor-ligand interactions (7–9) and various processes such as flow and chemical reactions (10,11).

The concept of FCS is based on the correlation analysis of fluorescence fluctuations in a confined observation volume. The sensitivity of the technique to detect binding of two or more components depends on the relative change in mass upon binding. For a multicomponent system consisting of reactants and products labeled with the same fluorescent dye, the only way of differentiating the product from the reactant is when the product has a molecular mass that differs from the reactants by a factor of at least 4–8 (12). This in turn shifts the correlation curve to higher diffusion times by up to a factor of 2 given by the Stokes-Einstein equation for spherical diffusing particles ($\tau_D \sim M^{1/3}$). By separately labeling the reactants with differently emitting fluorophores, the labels can be simultaneously excited with two different laser lines and detected in separate channels. The signals from both detector channels can then be cross correlated and the doubly labeled products easily distinguished from the singly labeled reactants independent of their mass. Earlier cross-correlation systems have made use of light scattering or a combination with fluorescence to measure their cross-correlation functions and determine rotational diffusion and association-dissociation dynamics (13,14). In dual-beam fluorescence cross-correlation spectroscopy, the setup consisting of two spatially separated focal points has been applied to characterize flow systems (15). Dual-color fluorescence cross-correlation spectroscopy was first experimentally realized by Schwille et al. to measure nucleic acid hybridizations (16,17). The potential of this technique to effectively measure biomolecular interactions has expanded its applications to detecting PCR complexes (18), monitoring enzyme kinetics (19,20), measuring protein-DNA interactions (21), and the analysis of live cells (22,23). Cross correlation has also been combined with FCS and Förster resonance energy transfer (FRET) for global data analysis (24). Two-photon excitation laser sources have been used to overcome the difficulty of aligning two laser beams to the same confocal volume (25). Increased axial resolution from a more confined focal spot reduces background fluorescence and photobleaching making it suitable for in vivo studies (26,27). Recently, two-photon excitation has achieved the

Submitted September 8, 2005, and accepted for publication April 5, 2006.

Address reprint requests to Dr. Thorsten Wohland, Tel.: 65-6516-1248; Fax: 65-6779-1691; E-mail: chmwt@nus.edu.sg.

0006-3495/06/07/715/13 $2.00

doi: 10.1529/biophysj.105.074120

excitation of up to three dyes simultaneously to perform triple-color coincidence analysis (28). However, the high cost of a high power femtosecond laser source and lower emission rates limit its potential applications. A less expensive method is the excitation of two or more fluorescent dyes by one-photon excitation with single laser wavelength by using dyes with similar excitation spectra but spectrally different emission characteristics. With the recent advent of long Stokes shift fluorophores such as nanocrystal quantum dots (29,30) and tandem dyes (31,32) or MegaStokes dyes (www.dyomics.com), multicolor imaging using a single laser wavelength for excitation has been achieved (33). Using single excitation wavelength in dual color fluorescence cross-correlation spectroscopy (SW-FCCS) was realized by Hwang and Wohland (34) to detect ligand-receptor binding. The resolution of SW-FCCS was explored by using dyes with similar emission characteristics such as fluorescein and tetramethylrhodamine (35).

In this article, we present an extension of this technique to multicolor SW-FCCS. Using a single laser wavelength to excite up to three differently emitting dyes simultaneously, we measured the binding of green ligand biotin-4-fluorescein (BF) and yellow ligand R-phycoerythrin biotin (BPE) to red receptor Alexa Fluor 647-R-phycoerythrin-streptavidin (AXSA). We formulated a theory to explain the pairwise cross correlations green × red ($G_{gr}(\tau)$), yellow × red ($G_{yr}(\tau)$), and green × yellow ($G_{gy}(\tau)$) for this system. For ways to extend the theory to take into account the sample impurities and labeling ratios, refer to Weidemann (36) and Hwang (35). It is shown that even with a higher amount of cross talk between three differently emitting fluorescent labels all excited at the same wavelength, SW-FCCS is capable of discriminating bound complexes from free reactants by more than 6 SD difference in the cross-correlation amplitudes. The capability of distinguishing trimers, dimers, and monomers regardless of their molecular weight, when performed with appropriate negative controls, opens up new possibilities of studying higher order interactions in complex molecular systems.

THEORY

Cross correlation of triple species

Fluorescence correlation spectroscopy involves the statistical analysis of fluorescence fluctuations coming from an illuminated observation volume. These fluctuations may arise from fluorescently labeled molecules undergoing different processes such as Brownian motion, fast transition between singlet and triplet states, and receptor-ligand interactions. Fluorescence signals $F_i(t)$ and $F_j(t)$ in detector channels i and j are correlated according to the normalized correlation function

$$G_{ij}(\tau) = \frac{\langle \delta F_i(t)\delta F_j(t+\tau)\rangle}{\langle F_i(t)\rangle\langle F_j(t)\rangle} = \frac{\langle F_i(t)F_j(t+\tau)\rangle}{\langle F_i(t)\rangle\langle F_j(t)\rangle} - 1, \quad (1)$$

where $i = j$ for autocorrelation of a single detector channel and $i \neq j$ for cross correlation of two channels.

In the following we assume we have a system consisting of R, a red fluorescent receptor with multiple binding sites for one ligand, and L_g and L_y, the ligand that is either labeled with a green or yellow emitting fluorophore. Considering a solution of receptor and ligands, free ligands L_f will bind with free receptors R_f to form complex RL_n at equilibrium binding where n is the number of bound ligands on R. We assume here that each complex formed consists of one receptor with several ligands specifically bound, therefore excluding oligomerization of this receptor.

$$\begin{aligned} R_f + L_f &\rightleftharpoons RL \\ RL + L_f &\rightleftharpoons RL_2 \\ &\dots \\ RL_{n-1} + L_f &\rightleftharpoons RL_n. \end{aligned}$$

We assume that each binding site has the same affinity. If we disregard the multiplicity of the binding sites, the dissociation constant K_d for each individual binding site is then given by the concentration of reactants divided by the products,

$$K_d = \frac{R_f \times L_f}{RL} = \frac{RL \times L_f}{RL_2} \dots = \frac{RL_{n-1} \times L_f}{RL_n}. \quad (2)$$

To take account of the multiple binding sites per receptor, binomial coefficients are introduced to describe the possibility of n ligands binding to n_t binding sites (37). The concentrations of free receptors and ligands are thus related to the total concentrations of receptor R_t and ligand L_t minus the sum of all bound receptors and ligands, respectively.

$$R_f = R_t - \sum_{n=1}^{n_t} \binom{n_t}{n} RL_n \quad (3)$$

$$L_f = L_t - \sum_{n=1}^{n_t} n\binom{n_t}{n} RL_n. \quad (4)$$

The concentrations of the complexes RL_n, L_f, and R_f at binding equilibrium can then be numerically determined by simultaneously solving Eqs. 2–4.

The total concentration of ligand L_t consists of the ligands L_g and L_y. The probability of encountering either ligand L_g or L_y to form a complex with a receptor is given by their mol fractions

$$f_{L_g} = \frac{L_g}{L_t}, \quad (5)$$

$$f_{L_y} = \frac{L_y}{L_t} = 1 - f_{L_g}. \quad (6)$$

Consider a receptor with n_t binding sites and n fluorescent ligands bound, of which n_g are L_g ligands and n_y are L_y ligands ($n_g \leq n \leq n_t$). In this case we have to account for the number of possibilities how to distribute firstly n ligands over n_t binding sites and secondly n_g ligands L_g to the n bound sites. The distribution of n_y ligands L_y to the n_y (= n −

n_g) remaining binding sites has then only one possibility. The concentration of a complex with n bound ligands becomes

$$RL_{(n,n_g)} = \binom{n_t}{n}\binom{n}{n_g} f_{L_g}^{n_g} \times f_{L_y}^{n_y} \times RL_n. \quad (7)$$

The first binomial coefficient describes the distribution of n bound ligands over the total number of binding sites n_t and the second coefficient is the distribution of L_g over the total number of bound ligands. Equations 3–7 will be used to calculate the cross-correlation amplitude as shown below.

The time dependent total fluorescence signal $F_i(t)$ in detection channel i is the sum of all fluorescent species ($s = L, R, RL$) contributing to the signal. It is determined by their fluorescence yields Q_s^i (often expressed as counts per molecule per second), and the time dependent number of particles $N_A V_{eff} C(t)$ in the effective observation volume V_{eff}. N_A is Avogadro's number and $C(t)$ represents the time-dependent values of the averages R_f, L_f, or $RL_{(n,n_g)}$ as defined in Eqs. 3, 4, and 7, respectively. All possible species that contribute with Q_s^i via cross talk into the detection channels are taken into account.

$$\begin{aligned} F_i(t) &= F_L^i(t) + F_R^i(t) + F_{RL}^i(t) \\ &= N_A V_{eff}\left[Q_L^i L_f(t) + Q_R^i R_f(t) + \sum_{n=1}^{n_t}\sum_{n_g=0}^{n} Q_{RL}^i RL_{(n,n_g)}(t)\right] \\ &= N_A V_{eff}\left[(Q_{L_g}^i f_{L_g} + Q_{L_y}^i f_{L_y})L_f(t) + Q_R^i R_f(t) + \sum_{n=1}^{n_t}\sum_{n_g=0}^{n}(n_g q_{L_g} Q_{L_g}^i + n_y q_{L_y} Q_{L_y}^i + Q_R^i)RL_{(n,n_g)}(t)\right]. \end{aligned} \quad (8)$$

The first term represents the total free ligands with different fluorescence yields Q_{Lg}, Q_{Ly} for ligands labeled with different fluorophores. The second term represents the free receptor and the third term denotes the complex itself with both types of ligands bound to the receptor where the fluorescence yield contribution of L_g and L_y are proportional to the number of ligands bound; i.e., $n_g \times QL_g$ and $n_y \times QL_y$. Changes in fluorescence yields upon binding via processes such as quenching or FRET are taken into account by the factors q_{Lg}, q_{Ly} where $q = 1.0$ if there is no change in fluorescence yield. Assuming that the emission spectra do not undergo any shifts in wavelength, q_{Lg}, q_{Ly} are the same in all channels.

Because we are only interested in observing relative changes in the cross-correlation amplitudes we calculate the cross-correlation function at $\tau = 0$. The fluorescence yield factor Q_s^{ij} is obtained by the product of fluorescence yields in the cross-correlated channels. It determines the weighting factor contributing from various species to the cross-correlation amplitude, respectively

$$Q_L^{ij} = Q_{L_g}^i Q_{L_g}^j f_{L_g} + Q_{L_y}^i Q_{L_y}^j f_{L_y} \quad (9)$$

$$Q_R^{ij} = Q_R^i Q_R^j \quad (10)$$

$$Q_{RL(n,n_g)}^{ij} = (n_g q_{L_g} Q_{L_g}^i + n_y q_{L_y} Q_{L_y}^i + Q_R^i)(n_g q_{L_g} Q_{L_g}^j + n_y q_{L_y} Q_{L_y}^j + Q_R^j). \quad (11)$$

By substituting Eq. 8 for two detection channels $i \times j$ (where $i \times j$ can be any combination pair of detection channels) into the cross-correlation function in Eq. 1, and assuming a three-dimensional (3D) Gaussian illumination intensity profile, the cross-correlation amplitude then becomes

$$G_{ij}^{+}(0) = \frac{Q_L^{ij} L_f + Q_R^{ij} R_f + \sum_{n=1}^{n_t}\sum_{n_g=0}^{n} Q_{RL(n,n_g)}^{ij} RL_{(n,n_g)}}{N_A V_{eff}\left[\left(Q_L^i L_f + Q_R^i R_f + \sum_{n=1}^{n_t}\sum_{n_g=0}^{n} Q_{RL(n,n_g)}^{i} RL_{(n,n_g)}\right)\left(Q_L^j L_f + Q_R^j R_f + \sum_{n=1}^{n_t}\sum_{n_g=0}^{n} Q_{RL(n,n_g)}^{j} RL_{(n,n_g)}\right)\right]}, \quad (12)$$

where the effective volume V_{eff} is experimentally determined.

The cross-correlation function for the negative control does not include binding of ligand to receptor therefore only cross talk is contributing to the function

$$G_{ij}^{-}(0) = \frac{Q_L^{ij} L_t + Q_R^{ij} R_t}{N_A V_{eff}[(Q_L^i L_t + Q_R^i R_t)(Q_L^j L_t + Q_R^j R_t)]}. \quad (13)$$

Equation 12 is based on the assumption that both L_g and L_y bind to R to form a trimer. But in the case where only one type of ligand is bound to R and the other remains free, the cross-correlation amplitude will resemble the positive control function for the bound ligand and receptor and the negative control function for the free ligand. In this case we have two possible cases.

$$\text{Case 1}: R + L_g + L_y \rightarrow RL_g + L_y.$$

In the case where all ligands binding to the red receptor R are green ligands L_g ($n = n_g$) and the yellow ligands L_y

remain free, the probability of binding L_g becomes 1. The concentration of complex RL_g from Eq. 7 becomes

$$RL_{(n_g)} = \binom{n_t}{n_g} RL_{n=n_g}. \quad (14)$$

All of the complexes formed consist of only RL_g, therefore there is no fraction of L_y contributing to the concentration of free ligands L_f after binding ($f_{Ly} = 0$) nor to the formation of the complex RL_g. Instead, all of L_y ($= f_{Ly}L_t$) remains as completely free ligands but still contribute to the cross-correlation function between $g \times r$ via cross talk. These conditions are substituted into the cross-correlation function in Eq. 12 to obtain $G_{ij}(0)$ as a positive control for $g \times r$

$$G_{ij}(0) = \frac{Q^{ij}_{L_g}L_f + Q^{ij}_{L_y}L_y + Q^{ij}_{R}R_f + \sum_{n_g=1}^{n_t} Q^{ij}_{RL(n_g)}RL_{(n_g)}}{N_A V_{eff}\left[\left(Q^{i}_{L_g}L_f + Q^{i}_{L_y}L_y + Q^{i}_{R}R_f + \sum_{n_g=1}^{n_t} Q^{i}_{RL(n_g)}RL_{(n_g)}\right)\left(Q^{j}_{L_g}L_f + Q^{j}_{L_y}L_y + Q^{j}_{R}R_f + \sum_{n_g=1}^{n_t} Q^{j}_{RL(n_g)}RL_{(n_g)}\right)\right]}. \quad (15)$$

The first two terms in the numerator denote free L_g and total nonbinding L_y, respectively. The third and fourth terms represent the contribution from free R and complexes RL_g, respectively. The fluorescence yield factors Q^{ij}_s for species s (where $s = L_g$ or L_y or R) are described by

$$Q^{ij}_s = Q^{i}_s Q^{j}_s \quad (16)$$

$$Q^{ij}_{RL(n_g)} = (n_g q_{L_g} Q^{i}_{L_g} + Q^{i}_{R})(n_g q_{L_g} Q^{j}_{L_g} + Q^{j}_{R}). \quad (17)$$

Because there are no bound complexes formed between L_g and L_y or R and L_y, $G_{gy}(0)$ and $G_{yr}(0)$ represent the negative controls and any contribution from the RL_g ligand-receptor complexes comes via cross talk.

$$\text{Case 2}: \; R + L_y + L_g \rightarrow RL_y + L_g.$$

In the case where all ligands bound to red R are yellow L_y ($n = n_y$) and green L_g remain free, the probability of binding L_y becomes 1. Equation 14 then refers to the concentration of complex RL_y formed and the cross correlations can be derived from Eqs. 15–17 by exchanging indices g and y.

Application of theory to biotin-streptavidin binding system

The biochemical system we present here consists of the red AXSA receptor R with up to four specific binding sites ($n_t = 4$) for biotin ligand that is differently labeled with fluorescein (L_g) and R-phycoerythrin (L_y). In this case, we vary the number of n_g and n_y ligands bound to R from 0 to 4, such that the complex is always at full binding with all streptavidin binding sites occupied with biotin (see Materials and Methods). The cross-correlation functions for the positive and negative controls G_{ij} can be any permutations of detection channels in the green, yellow, and red, corresponding to the colors at the emission maximum of the binding species.

MATERIALS AND METHODS

Optical setup

The SW-FCCS optical setup (Fig. 1) consisted of a CW Argon ion laser (Lasos Lasertechnik GmbH, Jena, Germany) with two laser lines 488 and 514 nm. An excitation filter z488/10× (Chroma Technology, Rockingham, VT) is used to transmit only the 488-nm excitation line. The collimated laser beam is expanded by two biconvex lenses $f = 10$ mm and $f = 150$ mm and illuminates the back aperture of a 40×/1.15 NA water immersion objective (Olympus, Hamburg, Germany) mounted on an Olympus microscope IX70. The beam is focused to a diffraction-limited spot in a sample solution containing fluorescent dyes. The emitted fluorescence is collected by the same objective and is transmitted by a dichroic mirror 505DRLP (Omega Optical, Brattleboro, VT), which separates the fluorescence from the scattering and excitation light. Two more dichroic mirrors 560DRLP and 630DRLP (Omega) split the emission pathway into three detection channels: green, yellow, and red. The intermediate focus by the tube lens is imaged (magnification $M = 1$) via three Achromat lenses $f = 30$ mm (green), 40 mm

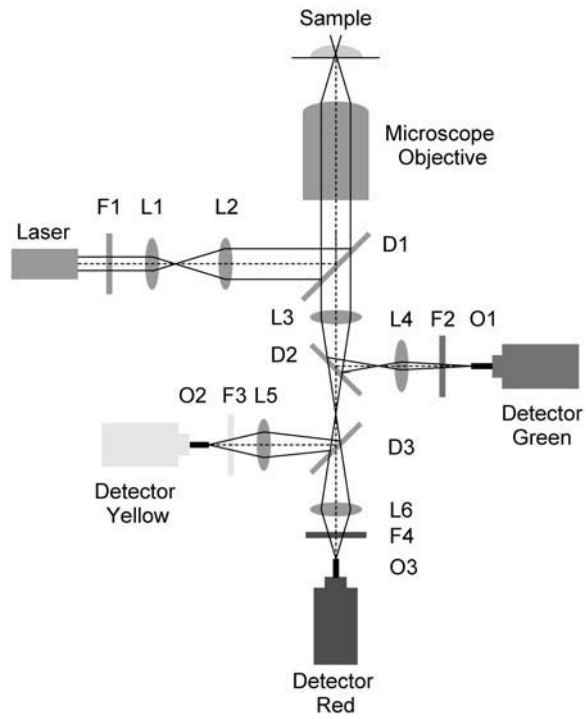

FIGURE 1 The three-color cross-correlation fluorescence spectrometer consists of a typical FCS setup with three detection pathways. A single laser beam is expanded and collimated by lenses L1 and L2. The microscope objective focuses the beam into the sample. The fluorescence light emitted is focused by the tube lens L3 and split three ways into different wavelength regions via dichroics D2 and D3. Lenses L4–L6 focus the emission beams onto fibers O1–O3. F1, excitation filter; F2–F4, bandpass filters; L1–L6, lenses; D1–D3, dichroic mirrors; O1–O3, optical fibers.

(yellow), and 50 mm (red) (Thorlabs, Newton, MA) onto the proximal end of a 50-μm fiber (Thorlabs). Bandpass filters 520DF40 (Omega), HQ585/40m and HQ700/90m (Chroma) are placed in front of the fiber ends to further restrict the wavelength interval for an enhanced wavelength filtering. Photons are detected with three avalanche photodiodes (Perkin-Elmer SPCM-AQR-13 in the green and yellow channel and SPCM-AQR-14 in the red channel). The signals are split between three hardware correlator cards Flex02-12D, Flex99 (Correlator.com, Bridgewater, NJ), and three pairwise cross correlations between green and red, yellow and red, and green and yellow channels are performed at the same time on three separate personal computers.

Chemistry

Ligands biotin-4-fluorescein, R-phycoerythrin biotin-XX conjugate and receptor Alexa Fluor 647-R-phycoerythrin-streptavidin were purchased from Invitrogen (Basel, Switzerland). Streptavidin is a homotetrameric protein with four biotin-binding sites. To maintain AXSA always at full binding with varying BF and BPE concentrations, 9 aliquots of AXSA was fixed at constant concentration 5 nM whereas BF was added in increasing concentrations from 0 to 20 nM to give BF/AXSA concentration ratios = 0, 0.5, 1...4. This was incubated before adding decreasing concentrations of BPE into the same aliquots from 20 to 0 nM at BPE/AXSA concentration ratios = 4, 3.5, 3...0 to fully occupy the remaining free binding sites of AXSA. Three types of negative controls with all three reactants at the same concentrations as the positive control were prepared in 9 aliquots to inhibit (1) all binding sites, (2) BPE binding, and (3) BF binding. Negative control (1) was prepared by first incubating AXSA with excess unlabeled D-biotin (Invitrogen, 1 μM) to saturate completely all binding sites then adding BF and incubating it before adding in BPE. In negative control (2), BPE binding was inhibited by first incubating BF with AXSA and then saturating all available binding sites with excess D-biotin (1 μM) before mixing BPE. Likewise, negative control (3) was prepared by first incubating BPE to AXSA and the remaining binding sites saturated with excess D-biotin (1 μM) before adding the inhibited BF ligand. All incubation times were ~30 min and all samples were prepared in PBS buffer pH 7.4 (Sigma-Aldrich Chemie GmbH, Buchs, Switzerland).

RESULTS AND DISCUSSION

Characterization of fluorophores for SW-FCCS

The fluorophores used for SW-FCCS have to be selected based on several criteria. First, they have to have largely different Stoke's shifts for minimal emission spectral cross talk in the detection channels. Second, the fluorophores have to have similar excitation characteristics where they can be optimally excited at the same laser wavelength and power with negligible photobleaching. A suitable set of dichroics and emission filters has to be chosen to match the maximum emission wavelengths of the fluorophores while reducing cross talk.

In this work, fluorescein, R-phycoerythrin, a 240-kDa phycobiliprotein, and Alexa Fluor 647-R-phycoerythrin, a tandem dye, were selected for SW-FCCS due to their overlapping excitation spectra and minimal cross talk. Tandem dyes are shorter wavelength emitting dyes such as phycobiliproteins linked to a red emitting dye, e.g., Alexa Fluor 647 or Cy5. They are excited at 488 nm and due to strong fluorescence energy transfer between the proteins and the red emitting dyes; emission is mainly detected in the red. Their molar extinction coefficients at 488 nm are shown in Table 1. The series of installed dichroic mirrors and bandpass filters effectively separates the emission wavelengths yet provide high count rates. Their absorbance and emission spectra are shown in Fig. 2, *A* and *B*. The fluorescence yields Q in each channel were calculated from the photon counts per second divided by the number of molecules determined from the amplitude of the autocorrelation function. The Q-values were corrected for background from Raman scattering of water in the yellow and Rayleigh scattering of the laser line (Table 1).

The quenching of BF and BPE upon binding was measured independently by adding excess unlabeled streptavidin (Sigma-Aldrich) and by monitoring the changes in their fluorescence intensities. The average fluorescence intensity for BPE remains the same ($q = 1.0$) upon binding streptavidin but BF is quenched 83% ($q = 0.17$) corresponding to literature values (38). Note that the shorter biotin-4-fluorescein ligand is quenched more than fluorescein-biotin (~75%) due to stronger, faster, and noncooperative binding between the less hindered biotin-4-fluorescein and streptavidin (38). The fluorescence yields Q and the quenching factors q in all three channels contributed by the fluorophores are tabulated in Table 1. These values are used to calculate the fits from Eq. 12 for the positive control curves. Average photon count rates detected for all three channels were measured and compared between the positive and negative controls for all binding ratios (data not shown). There were no relative changes observed in fluorescence intensities upon binding to form BPE-AXSA and BF-BPE complexes; therefore, FRET was excluded from the equations.

Other fluorophore combinations have also been considered for SW-FCCS. Organic dye pairs and quantum dots have been measured previously with this technique (34,35). In particular, quantum dots have become a convenient choice for multicolor detection due to high quantum yield and continuously tunable emission spectra that can all be excited with one laser line. In these experiments, organic dyes were selected instead of quantum dots due to the relative ease of control of binding ratios of biotin to streptavidin. Commercially available quantum dots are developed mainly for imaging purposes and usually have high protein to label conjugation (10–15 streptavidin molecules to 1 quantum dot), making the binding concentrations difficult to manipulate between three binding partners. In addition, aggregation problem with quantum dots has been previously

TABLE 1 Molar extinction coefficients ε at 488 nm, fluorescence yields (Q) in Hz/molecule and residual fluorescence factor (q) after binding of the receptor and ligands measured at a laser power of 50 μW

Molecule	ε [$M^{-1}cm^{-1}$]	Q (green)	Q (yellow)	Q (red)	q
BF	63,500	13,300	4300	500	0.17
BPE	824,500	200	24,400	2300	1.0
AXSA	980,000	6100	22,000	318,100	1.0

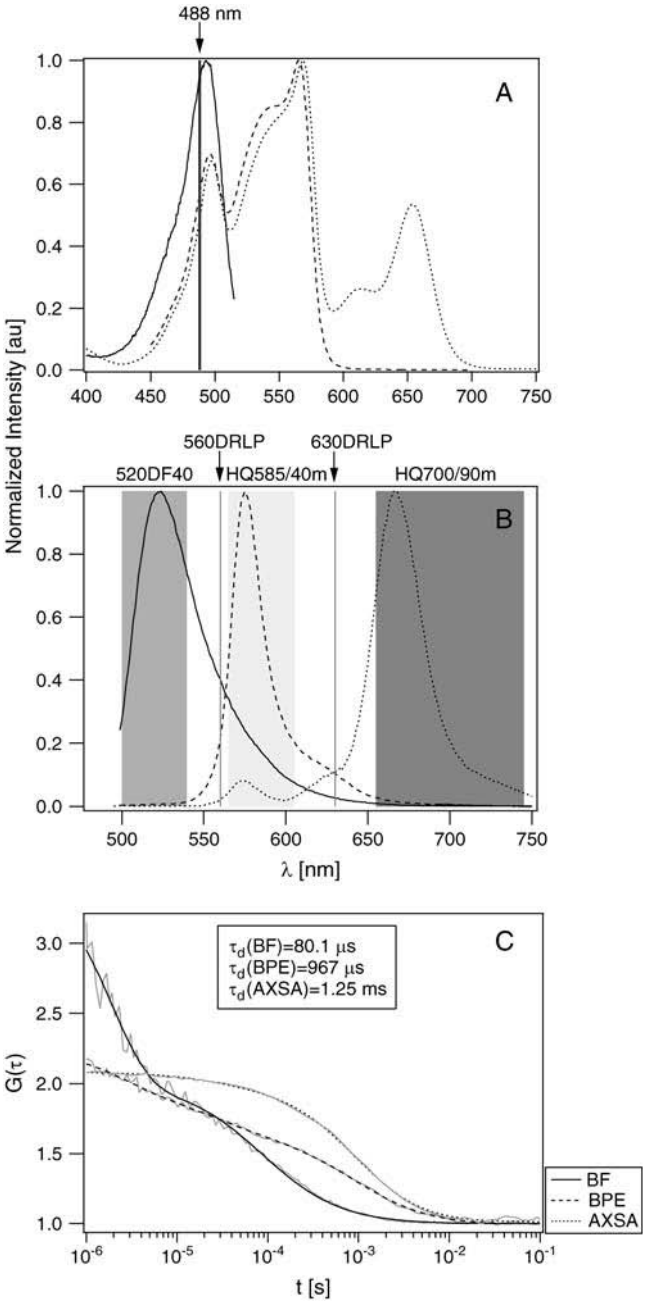

FIGURE 2 (*A*) Absorbance spectra of the fluorophores labels of BF, BPE, and AXSA. The excitation probabilities at the laser excitation line 488 nm are 93%, 56%, and 50%, respectively. (*B*) Fluorescence emission spectra of the three dyes. The detection windows of the molecules are specified by the dichroics and bandpass filters selected. All spectral curves are normalized. (*C*) Autocorrelation functions (*gray curves*) and their fits (*black curves*) all normalized to their total number of molecules in the green, yellow, and red detection channels for BF, BPE, and AXSA, respectively. The inset box shows the average diffusion times obtained from the fitting of the functions.

reported (34). Thus although quantum dots are better in terms of photostability and brightness, their aggregation in solution makes it difficult to unambiguously determine interactions. Alternatively, tandem dyes have been widely used in flow cytometric applications for simultaneous detection of multiple fluorophores excited with a single laser. We use these bright dyes for the same advantages for the application to SW-FCCS.

The large sizes of phycobiliproteins may pose problems as labels for smaller-sized target biomolecules. Therefore, a range of other possible dyes that could be used for in vitro and in vivo SW-FCCS, including fluorescent proteins and Megastokes dyes, have been measured. Their fluorescence yields in the different channels are listed with their filter sets in the Supplementary Material.

Calibration experiments

Calibration measurements were performed with Fluorescein (Invitrogen, 1 nM) in the green and yellow channels and AXSA in the red channel. Autocorrelation functions of BF, BPE, and AXSA were measured with increasing laser power from 50 to 500 μW to investigate the change of photon count rates per particle and triplet state population against excitation intensity. The diffusion times of the different molecules showed deviations at higher excitation intensities; however, this change depended on the molecular species and was minimal in our setup below 100 μW for all three species. The laser power of 50 μW was selected for minimal optical saturation and photobleaching of the dyes, as well as optimal count rates and low triplet fraction obtained between all three fluorescent dyes. Ten correlation functions measured for 10s were taken for all auto and cross-correlation functions. All correlation curves were fitted with the Levenberg-Marquadt fitting algorithm in Igor Pro (v4.0 Wavemetrics, Portland, OR). A fitting model for one-component diffusion model with triplet state (39) was used for the autocorrelation curves of BF and AXSA. The BPE autocorrelation curves were fitted with the one-component diffusion model with two triplet states where the first decay corresponds to the singlet-triplet lifetime in the microsecond timescale (40). The second decay in the tens of microseconds timescale could be due to other photodynamic process involved with R-phycoerythrin. The normalized autocorrelation functions and their fits are shown in Fig. 2 *C*. Fluorescein with a relative molecular weight of 376.3 Da and a reported diffusion coefficient D of 3.0×10^{-6} cm^2/s (6) was used as a standard dye to characterize the excitation volume. The beam waist radius w_o of 0.29 μm is calculated from the equation $w_o^2 = 4D\tau_d$ where the average diffusion time τ_d of 70.6 μs of fluorescein was determined from the fits of the autocorrelation functions. The diffusion coefficients of BF, BPE, and AXSA at 2.6×10^{-6} cm^2/s, 2.2×10^{-6} cm^2/s, and 1.7×10^{-7} cm^2/s, respectively, are calculated from the beam waist and the respective diffusion times that are obtained from the fits in Fig. 2 *C*. The relative molecular weights of the molecules are then determined from the Stokes'-Einstein equation, which assumes spherical molecules, to be 547.6 Da, 964 kDa, and 2,100 kDa, respectively. The experimentally determined

relative molecular weight of BF is similar to the literature value of 644.7 Da. However, the molecular weights of BPE and AXSA are much higher than the reported values of 240 and 294 kDa. This is most likely due to the nonspherical shapes of the molecules (41) that the equation does not take into account. A deviation from the spherical shape will lead to a decrease in the diffusion coefficient (9).

The blinking times of the triplet states for different labels are uncorrelated to each other despite being bound to the same complex. Thus, the triplet fractions that are detected in the autocorrelation functions are not detectable in the cross-correlation functions. The triplet state will reduce the count rate of the dye but the total number of molecules in the auto/cross-correlation functions remains constant. All the cross-correlation functions could be fitted sufficiently well with the one-component diffusion model and the structure parameter K (6) was obtained as 1.02 ± 0.02 for $G_{gr}(\tau)$, 1.06 ± 0.18 for $G_{yr}(\tau)$, and 3.45 ± 1.45 for $G_{gy}(\tau)$. The average K parameter was then fixed at 2 for all future cross-correlation fits.

Experimental results of biotin-streptavidin binding

In the following discussion, we will refer to AXSA as R, BPE as L_y, and BF as L_g. In general the cross-correlation functions exhibit the following trends. Under otherwise equal conditions the positive controls will have higher cross-correlation amplitudes due to complexes with multiple colors than the negative controls. The negative controls show only weak cross correlations due to the cross talk of the fluorophores into different channels. But both negative and positive controls will show decreasing amplitudes with increasing numbers of complexes or ligands and receptors.

Correlations of triple-color complexes

At any one time, three different components were mixed together in one sample aliquot and $G_{gr}(\tau)$, $G_{yr}(\tau)$, $G_{gy}(\tau)$ were measured simultaneously. The cross-correlation functions and their fits for a ligand/receptor concentration ratio $L_g/L_y/R = 2{:}2{:}1$ are shown in Fig. 3, *A–C*. The negative control amplitudes are due to cross talk between the respective channels but the positive control amplitudes are clearly higher due to the bound species. The amplitudes for each ligand/receptor ratio for positive and negative controls are plotted in Fig. 4, *A–C*. Fig. 4 *A* shows $G_{gr}(0)$ decreasing with 0–4 L_g and 4–0 L_y molecules bound to R due to the formation of complexes containing R and L_g (Eq. 12). In the case of the negative control (Eq. 13) where there is an absence of receptor-ligand complexes, the curve decreases sharply. The contribution to the amplitude is from cross talk, which is analogous to the autocorrelation curves. Likewise for Fig. 4 *B*, $G_{yr}(0)$ decrease toward increasing concentration of complexes containing R and L_y. Although there is no direct binding between L_g and L_y, the binding through an intermediate receptor R gives rise to $G_{gr}(\tau)$ as shown in Fig. 4 *C*. In this case, the positive control amplitude drops to a minimum toward the center of the curve where a maximum of complexes containing L_g and L_y is reached due to the presence of equal concentrations of L_g and L_y. As predicted, the correlation amplitudes are smaller for negative controls compared with positive controls in all cases.

Fitting analysis of triple-color complexes

It is well known that biotin-(strept)avidin has one of the strongest interactions known at present between a receptor and its ligand ($K_d = 10^{-15}$ M). To determine how accurate the fitting parameters are to model the experimental curves, we vary the parameters K_d and V_{eff} and determine the maximum values it can vary by changing the goodness-of-fit χ^2-value no more than 50% from the minimum best fit value. The negative control curves as shown by the shaded regions in Fig. 4, *A–C*, are fitted (Eq. 12) to give V_{eff} 1.1–2.1 femtoliters (Table 2). The fitted V_{eff} values generally increase with the emission wavelengths detected from the fluorescent dyes; i.e., $V_{eff}\ (G_{gy}(0)) \leq V_{eff}\ (G_{gr}(0)) \leq V_{eff}\ (G_{yr}(0))$. Positive controls are modeled with Eq. 12 to give the range of V_{eff} and K_d values (Table 2) as shown by the shaded regions in Fig. 4.

The obtained K_d values are well above the predicted 10^{-15} M. One reason for this is that the experiments were performed with sample concentrations in the nanomolar range (sensitivity limit of FCS), which makes it difficult to determine K_d values at six orders below this concentration limit. The K_d values determined from these fits, however, are close to FCS measurements done on the same binding system at similar concentration levels (42). Another reason could be due to ligand and/or receptor impurities that cause the binding curve to alter its slope. Labeling ratios between protein and label is another possible factor affecting the slope of the binding curve. Having more than one label increases the brightness of the product and this contributes to the autocorrelation amplitude with the square of its fluorescence yield and the cross-correlation function with the product of the fluorescence yields. Here we assume that all labeling ratios for ligands and receptor are 1:1 as stated by the supplier, and we use the average photon counts per particle per second to model the curves.

Nevertheless, it is the magnitude of difference in amplitudes between the positive and negative control curves that resolves the binding of two components. To determine complex formation, we demand that the difference between the positive (+) and negative (−) control should be at least 6 SD; i.e., $G^+(0) - G^-(0) \geq 3 * (SD^+ + SD^-)$. Factors that affect this difference include fluorescence yields, cross talk, and impurities (35). Although $G_{yr}(0)$ has a smaller difference because of larger cross talk between L_y and R from yellow emitting R-phycoerythrin molecules in R conjugates, the differences between all positive and negative control curves are more than 6 SD. Hence by measuring multiple cross-

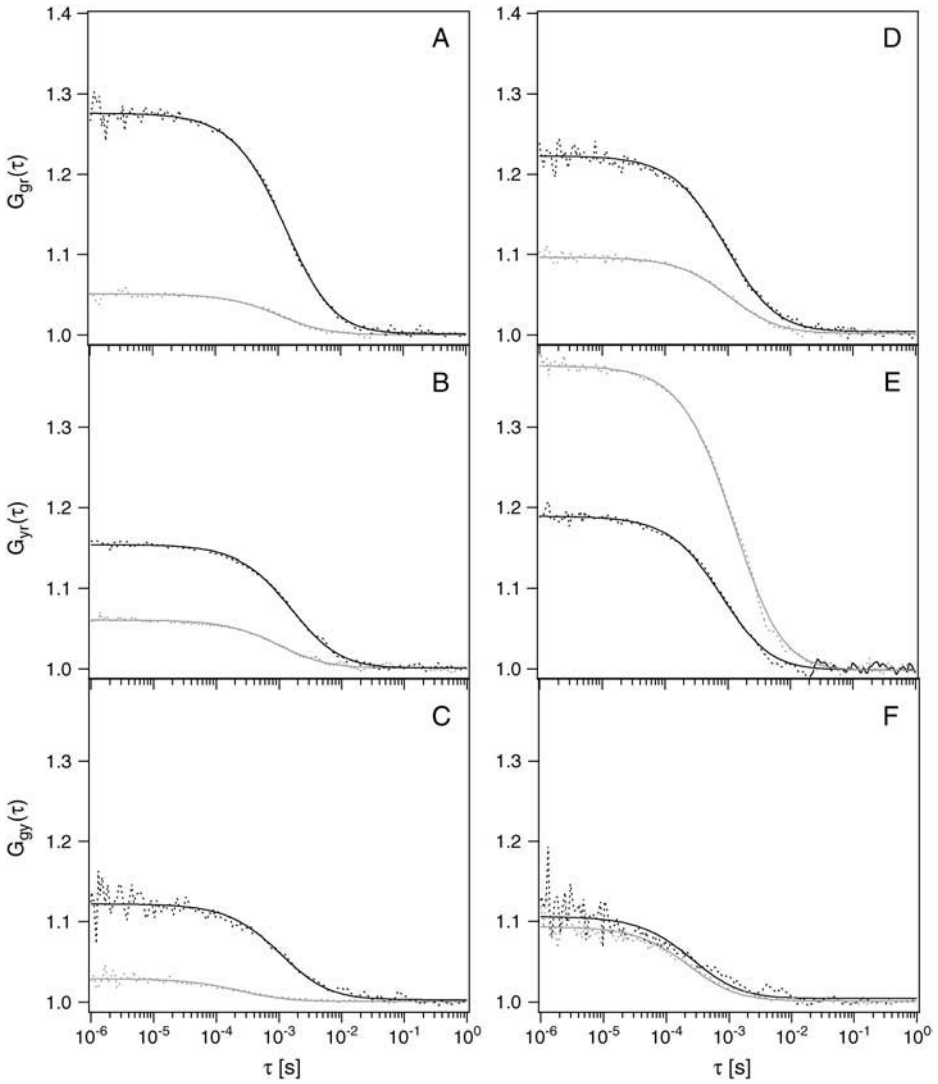

FIGURE 3 Cross-correlation functions of green × red, yellow × red, and green × yellow at concentration ratios $L_g/R = L_y/R = 2$ and $R = 5$ nM. (*A–C*) Positive control (*black curves*) and negative control (*gray curves*) of L_g and L_y binding to R. (*D–F*) Binding and inhibition curves of alternate ligand, L_g binding to R and L_y inhibited (*black curves*) or L_y binding to R and L_g inhibited (*gray curves*). Dotted curves show cross-correlation data and bold curves show their fits. Excitation wavelength, 488 nm; laser power, 50 μW.

correlation curves with a single sample at one $L_g/L_y/R$ concentration ratio, it is possible to determine binding between the different biomolecules.

The most significant difference between positive and negative controls are found when working at stoichiometric concentrations (see Supplementary Material). When measuring biotin/streptavidin ratios above 4:1 increasing free L_g molecules contribute larger background to the cross-correlation function, decreasing the amplitudes sharply toward the negative control, thus making binding irresolvable (35).

Correlations of complexes with alternate ligand binding

The difference in amplitudes between the positive and negative controls of Fig. 4, *A* and *B*, show that binding occurs between both L_g and L_y ligands with receptors. However, this does not prove the existence of complexes formed between L_g, L_y, and R simultaneously. Only $G_{gy}(\tau)$ confirms the existence of complexes containing L_g, L_y, and R. However, this conclusion is based on the assumption that the components are known beforehand and the nature of binding is identified. In this case, it is known that biotin binds specifically to streptavidin and does not dimerize with itself. In fact, $G_{gy}(\tau)$ may even be sufficient to determine complexation between L_g, L_y, and R here (43). In cases where the nature of binding is not known, additional negative controls will have to be performed to confirm that complexes RL_gL_y are formed. We have further performed these negative controls where only one ligand at a time is bound to the receptor and the binding of the second ligand is inhibited. The cross-correlation curves for a ligand/receptor concentration ratio of $L_g/L_y/R = 2{:}2{:}1$ are shown in Fig. 3, *D–F*. The binding and nonbinding cases are clearly distinguishable for $G_{gr}(\tau)$ and $G_{yr}(\tau)$ (Fig. 3, *D* and *E*) where the interacting species possess the higher cross-correlation amplitudes. The similar cross-correlation curves for $G_{gy}(\tau)$

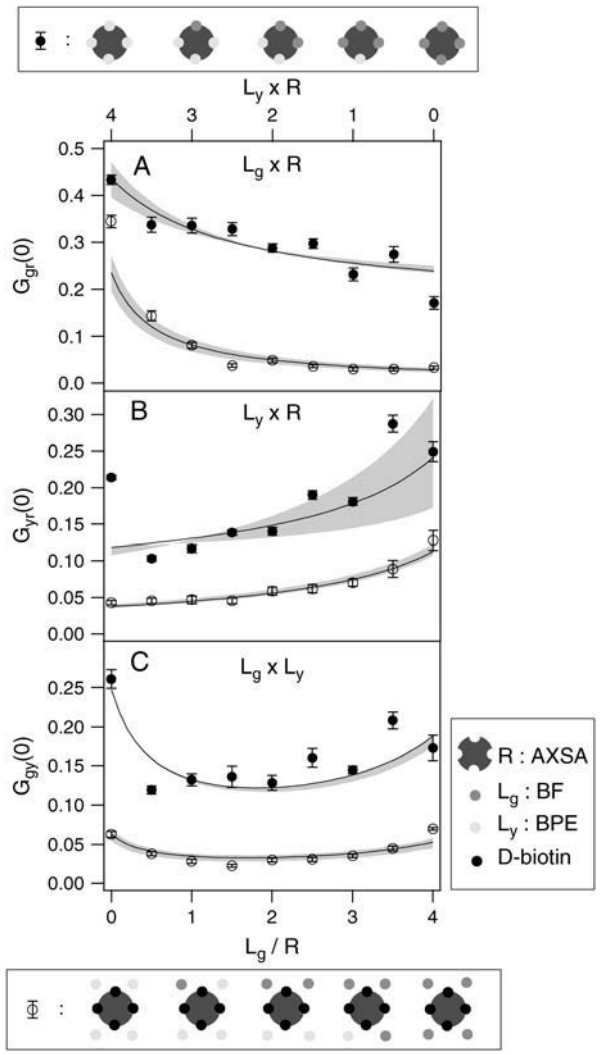

FIGURE 4 Simultaneous binding experiments of L_g and L_y ligands to R show the change of the cross-correlation amplitudes with increasing ligand/receptor concentration ratios. The top schematic drawing depicts R with four binding sites binding to 0–4 of L_g molecules and 4–0 of L_y molecules keeping the number of biotin ligands constant; and the bottom drawing depicts the negative control where all binding sites are inhibited with D-biotin. Experimental data points for positive control (*solid circles*) and negative control (*open circles*) show the binding between L_g and R (*A*); L_y and R (*B*), and L_g and L_y (*C*). The error bar at each data point is calculated from the standard deviation of 10 measurements. The black curve shows the best fitting model to the data points and the shaded regions show the K_d and V_{eff} limits where models are fitted within 50% of the minimum best fit parameter χ^2 (Table 2). The curves show a clear distinction between the positive and negative controls in their cross-correlation amplitudes. Excitation wavelength, 488 nm; laser power, 50 μW.

(Fig. 3 *F*) demonstrate that the ligands are not complexed either directly or indirectly via streptavidin. The cross-correlation amplitudes over the whole range of ligand/receptor ratios are plotted in Fig. 5, *A–C*.

Case 1: When L_g is added to R with L_y inhibited, $G_{gr}(0)$ (Fig. 5 *A*, *open circles*) decreases gradually comparable to the positive control (Fig. 4 *A*), whereas the $G_{yr}(0)$ and $G_{gy}(0)$ curves (Fig. 5, *B* and *C*, *open circles*) are similar to the negative controls of Fig. 4, *B* and *C*.

Case 2: Binding between L_y and R with L_g inhibited shows the $G_{yr}(0)$ values (Fig. 5 *B, solid circles*) eventually decreasing at higher L_y concentrations, as expected. Conversely, the $G_{gr}(0)$ and $G_{gy}(0)$ negative controls curves (Fig. 5, *A* and *C, solid circles*) decrease rapidly to lower amplitudes similar to the negative control curves in Fig. 4, *A* and *C*.

In Fig. 5 *A* the cross correlations $G_{gr}(0)$ have the same amplitudes when no ligand L_g is present. The same effect can be observed in Fig. 5 *B*, where the cross-correlation amplitudes are similar when no ligand L_y is present. For all other cases the cross correlations representing the interacting molecules are always higher in amplitude than the cross correlation representing the noninteracting molecules. In Fig. 5 *C*, the $G_{gy}(0)$ values are similar, no matter whether L_y or L_g is inhibited from binding. The curves are comparable to the negative control of Fig. 4 *C* because no complexes containing L_g and L_y simultaneously exist. In addition, it should be noted that if all three species are present, the amplitudes of the cross-correlation functions are always highest for the case of interacting molecules. For instance, when inhibiting L_y from binding (*open circles*) the highest amplitudes are found in Fig. 5 *A*, the $G_{gr}(0)$ channel. Conversely, when inhibiting L_g from binding (*solid circles*) the highest amplitudes are found in the $G_{yr}(0)$ channel (Fig. 5 *B*). The triple pairwise cross correlations directly show which molecules are interacting, thus substantiate the initial results from Fig. 4, *A–C*, that trimers are indeed formed between both ligands and the receptor.

Fitting analysis of complexes with alternate ligand binding

Additional negative control curves with L_y or L_g binding inhibited are also modeled with Eq. 15 to give the best fit range of V_{eff} and K_d within 50% of the lowest χ^2 (*shaded regions*, Fig. 5, *A–C*). The exception is the $G_{gr}(0)$ curve representing L_y binding and L_g inhibition (Fig. 5 *A*, *solid circles*), which could not be fitted to give K_d values within the limits of 10^{-15}–10^{-6} M. This is due to the fact that L_y does have negligible cross talk into the green channel (see Table 1) and thus the RL_y complexes do not contribute to the cross-correlation function and a determination of a K_d value is not possible. Therefore, the data points are fitted instead with Eq. 13 where cross talk from free L_y and RL_y complexes into the green channel could be taken to be negligible. The fitting analysis yield K_d values of biotin-streptavidin binding from 10^{-11} to 10^{-8} M (Table 2). The difference between $G_{gr}(0)$ positive and negative control curve is more than 6 SD (Fig. 5 *A*). This excludes the first point that does not have any L_g present and consists of only background from RL_y complexes. $G_{yr}(0)$ on the other hand fulfills the condition for binding only at higher concentrations of L_y/R (Fig. 5 *B*). This

TABLE 2 Lower to upper limits and best fit values obtained for effective observation volumes (V_{eff}) and equilibrium dissociation constants (K_d), determined from the various binding curves

Samples		V_{eff}		K_d	
		Lower to upper	Best fit	Lower to upper	Best fit
Negative control	$G_{gr}(0)$	1.3–1.8	1.5	–	–
	$G_{yr}(0)$	1.84–2.1	2.0	–	–
	$G_{gy}(0)$	1.1–1.4	1.2	–	–
Positive control	$G_{gr}(0)$	0.83–1.0	0.9	(2–4) 10^{-8}	1×10^{-8}
	$G_{yr}(0)$	0.7–1.57	1.0	(0.07–1.9) 10^{-8}	7×10^{-10}
	$G_{gy}(0)$	0.35–0.39	0.35	(2–7) 10^{-8}	4×10^{-8}
L_g +(L_y −)	$G_{gr}(0)$	0.94–1.1	1.0	(0.7–1) 10^{-8}	1×10^{-8}
	$G_{yr}(0)$	1.2–1.3	1.3	(0.05–1) 10^{-9}	5×10^{-11}
	$G_{gy}(0)$	2.5–3.1	3.1	(0.5–4) 10^{-10}	5×10^{-11}
L_y +(L_g −)	$G_{gr}(0)$	0.94–1.1	1.1	–	–
	$G_{yr}(0)$	1.63–2.2	2.2	(0.09–4) 10^{-9}	9×10^{-11}
	$G_{gy}(0)$	1.1–1.26	1.2	(5–7) 10^{-9}	6×10^{-9}

Bound (+); free (−).

is because at low L_y/R concentrations, free L_g molecules contribute to the cross correlation as background via cross talk, making binding indistinguishable. Both the negative controls with L_y or L_g inhibited have no contribution to $G_{gy}(\tau)$ from simultaneous binding of L_y and L_g to R (Fig. 5 *C*). Therefore both curves at low amplitudes show little difference from each other and the contribution to the cross-correlation amplitudes come mainly from cross talk of the fluorophores.

Limitations of SW-FCCS

Influence of K_d on cross correlations

The effect of K_d on cross-correlation amplitudes were calculated from the models as a function of ligand/receptor concentration ratios. K_d values were varied from 10^{-15} to 10^{-7} M at full binding conditions (Fig. 6, *A–C*). The changes in cross-correlation amplitudes of the negative control curves are due to cross talk in both channels. The positive control curves decrease toward higher ligand concentrations for Fig. 6, *A* and *B*, but remain relatively constant for Fig. 6 *C*. At higher K_d values (10^{-7} M) where more free reactants contribute to the cross-correlation functions and fewer complexes are formed, the separations of amplitudes between the positive and negative control curves diminish. Thus the limit of measurable K_d is reached when the positive and negative control have a difference that is smaller than 6 SD. This in turn is dependent on the count rates of the different reactants and their cross talk into the different channels.

Influence of impurities on cross correlations

Various types of impurities influence cross-correlation measurements. Inactive or unlabeled receptors or ligands contribute to the reduction in the difference between the positive and negative controls and decreases the sensitivity of the method. Multiple labeling sites on a reactant may as well affect the cross-correlation amplitudes. Some of these problems can be circumvented in cellular measurements when fluorescent proteins are used and labeling ratios are fixed. These parameters and its effects on dual-color SW-FCCS have been analyzed in detail (35).

Stoichiometry determination

The determination of stoichiometry with SW-FCCS has been demonstrated previously for direct binding with dual-color biomolecules (34,35). In this case for triple-color cross correlations, the ligands bind indirectly over a common interaction partner. With higher background due to an additional third color, the stoichiometry can still be determined in a similar way depending on the K_d values of the ligands. By varying each ligand L_g and L_y across a range of concentrations while maintaining the receptor concentration constant, a plot of $G^{+}_{gy}(0)$ with L_g and L_y will reveal the stoichiometry of the binding system. Various simulations of different stoichiometric ratios and further explanations are presented in the Supplementary Material.

Applications of multicolor SW-FCCS

The extension of FCCS to three colors diminishes the signal/noise ratio of the measurements because a narrower wavelength range is available for each channel and cross talk between the channels will be larger. Nevertheless, the extension to three colors is important for at least two reasons. Firstly, the biological variability between cells is often so high that any correlations between distinct biomolecules are hidden and can only be detected when all relevant molecules are observed simultaneously in a cell. Secondly, complex biochemical reactions in cellular systems involve higher order molecular interactions. These interactions consist of temporal association

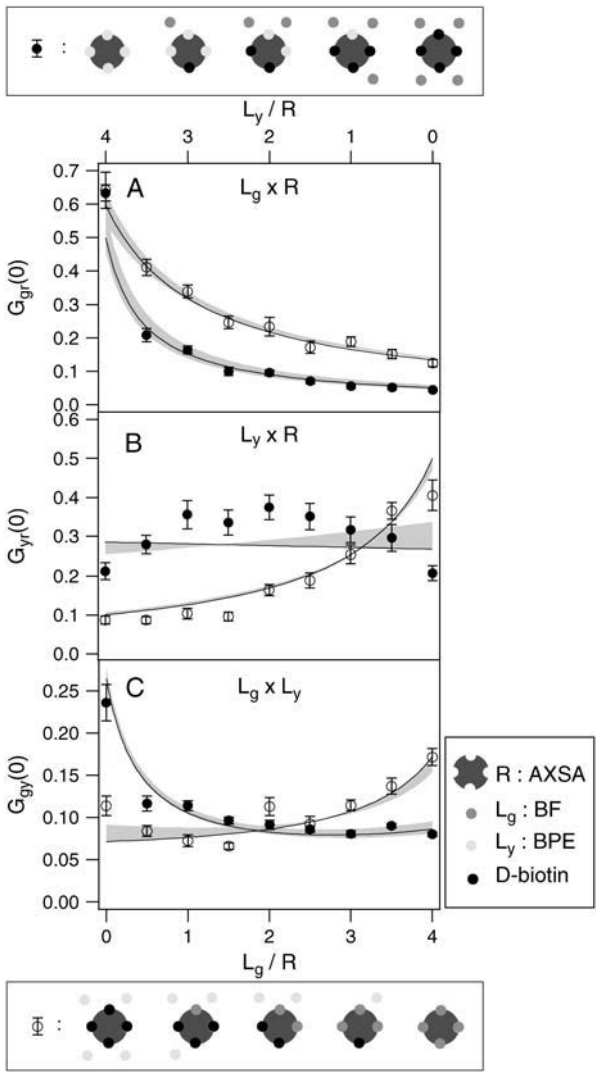

FIGURE 5 Controls with alternate ligand L_g or L_y inhibited independently with D-biotin are shown in the top and bottom schematic drawings, respectively. The cross-correlation amplitudes versus ligand/receptor concentration ratios are depicted. L_g bound and L_y free (*open circles*) give higher amplitudes for $G_{gr}(0)$ indicating RL_g complexes formed (*A*), but no binding shown for $G_{yr}(0)$ (*B*) and $G_{gy}(0)$ (*C*). The cross correlations with L_y bound and L_g free (*solid circles*) give higher amplitudes for $G_{yr}(0)$ indicating RL_y complexes formed (*B*), but no binding shown for $G_{gr}(0)$ (*A*) and $G_{gy}(0)$ (*C*). Black curves show the best fit curve with the lowest χ^2 and the shaded regions give the limits of K_d values and V_{eff} values fit to within 50% of the lowest χ^2 (Table 2). Excitation wavelength, 488 nm; laser power, 50 μW.

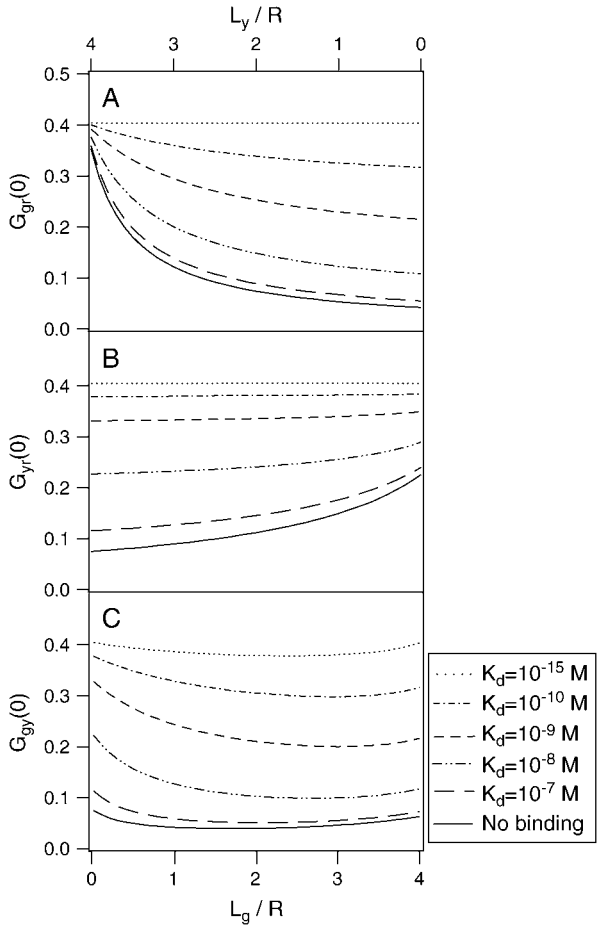

FIGURE 6 Effect of K_d on cross-correlation amplitudes calculated for the binding of L_g and L_y to R using fluorescence yields from Table 1 at $V_{eff} = 1.0$ fl and 4:1 stoichiometry. Cross-correlation amplitudes are plotted versus ligand/receptor concentration ratios for (*A*) $G_{gr}(0)$; (*B*) $G_{yr}(0)$, and (*C*) $G_{gy}(0)$. The positive control curves with lower binding affinity converge toward the negative control.

and dissociation reactions that multicolor SW-FCCS has the potential to detect and monitor. For instance, the detection of binding of the various proteins involved in signaling complexes in a cellular environment over time can only be followed when the different interaction partners are labeled. To be able to detect these intermediate complexes, the lifetimes of these complexes have to be longer than the time it takes for the complexed molecule to diffuse through the observation volume and the characteristic times of the interactions have to be of the same order or longer than our measurement time, which is limited by ~1 s for FC(C)S. If that is the case, SW-FCCS measurements with three colors can differentiate between trimers, dimers, and monomers and can elucidate temporal sequence of biological interactions.

CONCLUSION

In this study, we have performed fluorescence multicolor cross correlations using single laser wavelength for the excitation and simultaneous detection of three spectrally distinguishable fluorophores. The independent binding of two differently labeled ligands to a receptor tagged with a third color was verified with the standard biotin-streptavidin system. Modeling the positive control curves with the described FCCS theory enabled the determination of dissociation constants. Although several factors such as cross talk, impurities, and potential multiple labeling ratios limit the accurate determination of K_d from the positive control curves

compared with the literature value, we have shown that the method succeeds in resolving the different possible complexes of three interacting molecules.

Multicolor SW-FCCS provides a fast and convenient method to offer yes or no answers to interacting biochemical systems, determine an upper K_d limit, and determine the stoichiometry of binding. Existing FCS optical setups can be easily modified to perform SW-FCCS by including three detectors at the detection pathway while keeping the excitation path unchanged with one CW laser. Multiple laser excitation setups, in contrast, involve the complicated alignment of several laser beams in 3D to the same excitation volume and suffer from artifacts of nonideal overlap of excitation volumes that arise because of chromatic aberrations. Compared to multiphoton FCCS, SW-FCCS utilizes one-photon excitation that not only uses less expensive lasers but also offers higher count rates per particle and a better signal/noise ratio (44). In addition, recent advances in the setup of the detection pathways by using dispersive elements further simplify the setup and offer a simpler way of choosing wavelength ranges for detection and thus minimization of spectral cross talk (45,46).

SW-FCCS uses fluorophores that require similar excitation spectra but spectrally different emission characteristics with minimal cross talk. It has been shown to work with tandem dyes, quantum dots, and even with spectrally similar organic dyes. In Supplementary Material we give as well experimental count rates per particle for fluorescent proteins and small organic dyes with large Stokes shifts, both of which are potential fluorophores for this technique. The high sensitivity of FCS and its ability to probe spatial and temporal reactions coupled with the capability to detect multicolor labels simultaneously using single laser excitation, provides the opportunity to study higher order complex formation and molecular networks with a good signal/noise ratio in live cells. Potential applications include interactions involving membrane receptors, intracellular signaling proteins, and DNA transcription factors in signaling networks.

SUPPLEMENTARY MATERIAL

An online supplement to this article can be found by visiting BJ Online at http://www.biophysj.org.

We thank Horst Vogel and Ruud Hovius for discussions and assistance.

This work was supported by the Academic Research Fund of the National University of Singapore and funding from Ecole Polytechnique Fédérale de Lausanne.

REFERENCES

1. Magde, D., E. L. Elson, and W. W. Webb. 1972. Thermodynamic fluctuations in a reacting system: measurements by fluorescence correlation spectroscopy. *Phys. Rev. Lett.* 29:705–708.
2. Elson, E. L., and D. Magde. 1974. Fluorescence correlation spectroscopy. I. Conceptual basis and theory. *Biopolymers.* 13:1–27.
3. Koppel, D. E. 1974. Statistical accuracy in fluorescence correlation spectroscopy. *Phys. Rev. A.* 10:1938–1945.
4. Qian, H., and E. Elson. 1991. Analysis of confocal laser-microscope optics for 3-D fluorescence correlation spectroscopy. *Appl. Opt.* 30: 1185–1195.
5. Rigler, R., U. Mets, J. Widengren, and P. Kask. 1993. Fluorescence correlation spectroscopy with high count rate and low-background: analysis of translational diffusion. *Eur. Biophys. J.* 22: 169–175.
6. Thompson, N. L. 1991. Fluorescence correlation spectroscopy. *In* Topics in Fluorescence Spectroscopy, Vol. 1: Techniques. J. R. Lakowicz, editor. Plenum Press, New York. 337–378.
7. Rauer, B., E. Neumann, J. Widengren, and R. Rigler. 1996. Fluorescence correlation spectrometry of the interaction kinetics of tetramethylrhodamin α-bungarotoxin with *Torpedo califonica* acetylchoine receptor. *Biophys. Chem.* 58:3–12.
8. Van Craenenbroeck, E., and Y. Engelborghs. 1999. Quantitative characterization of the binding of fluorescently labeled colchicine to tubulin in vitro using fluorescence correlation spectroscopy. *Biochemistry.* 38:5082–5088.
9. Wohland, T., K. Friedrich, R. Hovius, and H. Vogel. 1999. Study of ligand receptor interactions by fluorescence correlation spectroscopy with different fluorophores: evidence that the homopentameric 5-hydroxytryptamine type 3As receptor binds only one ligand. *Biochemistry.* 38:8671–8681.
10. Gosch, M., H. Blom, J. Holm, T. Heino, and R. Rigler. 2000. Hydrodynamic flow profiling in microchannel structures by single molecule fluorescence correlation spectroscopy. *Anal. Chem.* 72:3260–3265.
11. Widengren, J., and R. Rigler. 1998. Review: fluorescence correlation spectroscopy as a tool to investigate chemical reactions in solutions and on cell surfaces. *Cell. Mol. Biol.* 44:857–879.
12. Meseth, U., T. Wohland, R. Rigler, and H. Vogel. 1999. Resolution of fluorescence correlation measurements. *Biophys. J.* 76:1619–1631.
13. Kam, Z., and R. Rigler. 1982. Cross-correlation laser scattering. *Biophys. J.* 39:7–13.
14. Ricka, J., and T. Binkert. 1989. Direct measurement of a distinct correlation-function by fluorescence cross-correlation. *Phys. Rev. A.* 39:2646–2652.
15. Brinkmeier, M., K. Dorre, J. Stephan, and M. Eigen. 1999. Two beam cross correlation: a method to characterize transport phenomena in micrometer-sized structures. *Anal. Chem.* 71:609–616.
16. Schwille, P., F. Meyer-Almes, and R. Rigler. 1997. Dual-color fluorescence cross-correlation spectroscopy for multicomponent diffusional analysis in solution. *Biophys. J.* 72:1878–1886.
17. Schwille, P. 2001. Cross-correlation analysis in FCS. *In* Fluorescence Correlation Spectroscopy: Theory and Applications. E. L. Elson and R. Rigler, editors. Springer, Berlin, Germany. 360–378.
18. Rigler, R., Z. Foldespapp, F. J. MeyerAlmes, C. Sammet, M. Volcker, and A. Schnetz. 1998. Fluorescence cross-correlation: a new concept for polymerase chain reaction. *J. Biotech.* 63:97–109.
19. Kettling, U., A. Koltermann, P. Schwille, and M. Eigen. 1998. Real-time enzyme kinetics monitored by dual-color fluorescence cross-correlation spectroscopy. *Proc. Natl. Acad. Sci. USA.* 95:1416–1420.
20. Rarbach, M., U. Kettling, A. Koltermann, and M. Eigen. 2001. Dual-color fluorescence cross-correlation spectroscopy for monitoring the kinetics of enzyme-catalyzed reactions. *Methods.* 24:104–116.
21. Rippe, K. 2000. Simultaneous binding of two DNA duplexes to the NtrC-enhancer complex studied by two-color fluorescence cross-correlation spectroscopy. *Biochemistry.* 39:2131–2139.
22. Bacia, K., I. V. Majoul, and P. Schwille. 2002. Probing the endocytic pathway in live cells using dual-color fluorescence cross-correlation analysis. *Biophys. J.* 83:1184–1193.

23. Saito, K., I. Wada, M. Tamura, and M. Kinjo. 2005. Direct detection of caspase-3 activation in single live cells by cross-correlation analysis. *Biochem. Biophys. Res. Commun.* 324:849–854.

24. Eggeling, C., P. Kask, D. Winkler, and S. Jager. 2005. Rapid analysis of Förster resonance energy transfer by two-color global fluorescence correlation spectroscopy: trypsin proteinase reaction. *Biophys. J.* 89: 605–618.

25. Heinze, K. G., A. Koltermann, and P. Schwille. 2000. Simultaneous two-photon excitation of distinct labels for dual-color fluorescence crosscorrelation analysis. *Proc. Natl. Acad. Sci. USA.* 97:10377–10382.

26. Berland, K. M., P. T. C. So, and E. Gratton. 1995. Two-photon fluorescence correlation spectroscopy: method and application to the intracellular environment. *Biophys. J.* 68:694–701.

27. Schwille, P., U. Haupts, S. Maiti, and W. W. Webb. 1999. Molecular dynamics in living cells observed by fluorescence correlation spectroscopy with one- and two-photon excitation. *Biophys. J.* 77:2251–2265.

28. Heinze, K. G., M. Jahnz, and P. Schwille. 2004. Triple-color coincidence analysis: one step further in following higher order molecular complex formation. *Biophys. J.* 86:506–516.

29. Alivisatos, A. P. 1996. Semiconductor clusters, nanocrystals, and quantum dots. *Science.* 271:933–937.

30. Grecco, H. E., K. A. Lidke, R. Heintzmann, D. S. Lidke, C. Spagnuolo, O. E. Martinez, E. A. Jares-Erijman, and T. M. Jovin. 2004. Ensemble and single particle photophysical properties (two-photon excitation, anisotropy, FRET, lifetime spectral conversion) of commercial quantum dots in solution and in live cells. *Microsc. Res. Tech.* 65:169–179.

31. Glazer, A. N., and L. Stryer. 1983. Fluorescent tandem phycobiliprotein conjugates. *Biophys. J.* 43:383–386.

32. Gruber, H. J., G. Kada, M. Marek, and K. Kaiser. 1998. Accurate titration of avidin and streptavidin with biotin- fluorophore conjugates in complex, colored biofluids. *Biochim. Biophys. Acta.* 1381:203–212.

33. Lacoste, T. D., X. Michalet, F. Pinaud, D. S. Chemla, A. P. Alivisatos, and S. Weiss. 2000. Ultrahigh-resolution multicolor colocalization of single fluorescent probes. *Proc. Natl. Acad. Sci. USA.* 97:9461–9466.

34. Hwang, L. C., and T. Wohland. 2004. Dual-color fluorescence cross-correlation spectroscopy using single laser wavelength excitation. *Chem. Phys. Chem.* 5:549–551.

35. Hwang, L. C., and T. Wohland. 2005. Single wavelength excitation fluorescence cross-correlation spectroscopy with spectrally similar fluorophores: resolution for binding studies. *J. Chem. Phys.* 122: 114708 (1–11).

36. Weidemann, T., M. Wachsmuth, M. Tewes, K. Rippe, and J. Langowski. 2002. Analysis of ligand binding by two-colour fluorescence cross-correlation spectroscopy. *Single Mol.* 3:49–61.

37. Tuk, B., and M. F. van Oostenbruggen. 1996. Solving inconsistencies in the analysis of receptor-ligand interactions. *Trends Pharmacol. Sci.* 17:403–409.

38. Kada, G., H. Falk, and H. J. Gruber. 1999. Accurate measurement of avidin and streptavidin in crude biofluids with a new, optimized biotin-fluorescein conjugate. *Biochim. Biophys. Acta.* 1427: 33–43.

39. Widengren, J., Ü. Mets, and R. Rigler. 1995. Fluorescence correlation spectroscopy of triplet states in solution: a theoretical and experimental study. *J. Phys. Chem.* 99:13368–13379.

40. Widengren, J., U. Mets, and R. Rigler. 1999. Photodynamic properties of green fluorescent proteins investigated by fluorescence correlation spectroscopy. *Chem. Phys.* 250:171–186.

41. MacColl, R., L. E. Eisele, E. C. Williams, and S. S. Bowser. 1996. The discovery of a novel R-phycoerythrin from an Antarctic red alga. *J. Biol. Chem.* 271:17157–17160.

42. Swift, J. L., R. Heuff, and D. T. Cramb. 2006. A two-photon excitation fluorescence cross-correlation assay for a model ligand-receptor binding system using quantum dots. *Biophys. J.* 90:1396–1410.

43. Berland, K. M. 2004. Detection of specific DNA sequences using dual-color two-photon fluorescence correlation spectroscopy. *J. Biotechnol.* 108:127–136.

44. Bacia, K., S. A. Kim, and P. Schwille. 2006. Fluorescence cross-correlation spectroscopy in living cells. *Nat. Methods.* 3:83–89.

45. Burkhardt, M., K. G. Heinze, and P. Schwille. 2005. Four-color fluorescence correlation spectroscopy realized in a grating-based detection platform. *Opt. Lett.* 30:2266–2268.

46. Hwang, L. C., M. Leutenegger, M. Gosch, T. Lasser, P. Rigler, W. Meier, and T. Wohland. 2006. Prism-based multicolor fluorescence correlation spectrometer. *Opt. Lett.* 31:1310–1312.